© 2016. Published by The Company of Biologists Ltd | Development (2016) 143, 54-65 doi:10.1242/dev.130005

RESEARCH ARTICLE

The development and plasticity of alveolar type 1 cells

Jun Yang[1,*], Belinda J. Hernandez[1,*], Denise Martinez Alanis[1], Odemaris Narvaez del Pilar[2], Lisandra Vila-Ellis[1,3], Haruhiko Akiyama[4], Scott E. Evans[1], Edwin J. Ostrin[1] and Jichao Chen[1,5,‡]

ABSTRACT

Alveolar type 1 (AT1) cells cover >95% of the gas exchange surface and are extremely thin to facilitate passive gas diffusion. The development of these highly specialized cells and its coordination with the formation of the honeycomb-like alveolar structure are poorly understood. Using new marker-based stereology and single-cell imaging methods, we show that AT1 cells in the mouse lung form expansive thin cellular extensions via a non-proliferative two-step process while retaining cellular plasticity. In the flattening step, AT1 cells undergo molecular specification and remodel cell junctions while remaining connected to their epithelial neighbors. In the folding step, AT1 cells increase in size by more than 10-fold and undergo cellular morphogenesis that matches capillary and secondary septa formation, resulting in a single AT1 cell spanning multiple alveoli. Furthermore, AT1 cells are an unexpected source of VEGFA and their normal development is required for alveolar angiogenesis. Notably, a majority of AT1 cells proliferate upon ectopic SOX2 expression and undergo stage-dependent cell fate reprogramming. These results provide evidence that AT1 cells have both structural and signaling roles in alveolar maturation and can exit their terminally differentiated non-proliferative state. Our findings suggest that AT1 cells might be a new target in the pathogenesis and treatment of lung diseases associated with premature birth.

KEY WORDS: Lung development, Cell plasticity, Alveolar angiogenesis

INTRODUCTION

The mammalian lung consists of a tree-like airway compartment and a honeycomb-like gas exchange compartment. The two major epithelial cell types covering the gas exchange compartment are alveolar type 1 (AT1) and type 2 (AT2) cells, which are in close contact with underlying capillaries and fibroblasts (Williams, 2003; Herzog et al., 2008; Weibel, 2015). AT1 cells are flat and cover more than 95% of the gas exchange surface, whereas AT2 cells are cuboidal and synthesize surfactants to prevent the alveoli from collapsing (Crapo et al., 1982; Williams, 2003). Classical electron microscopy studies show that AT1 cells are extremely thin (<0.1 µm), presumably to facilitate passive gas diffusion, and have a complex morphology that can be traced over multiple alveoli (Weibel, 1971, 2015). Whereas AT2 cells have recently been shown to self-renew and give rise to AT1 cells during homeostasis and injury repair (Barkauskas et al., 2013; Desai et al., 2014), AT1 cells are generally considered terminally differentiated *in vivo*, although they exhibit some plasticity in culture (Danto et al., 1995; Williams, 2003; Gonzalez et al., 2005, 2009). One recent study suggests that, although infrequent, AT1 cells may convert to AT2 cells and proliferate upon pneumonectomy or oncogenic KRAS expression (Jain et al., 2015).

During development, recent studies suggest that a population of bipotential progenitors expressing markers of both AT1 and AT2 cells differentiate into mature AT1 or AT2 cells by upregulating additional markers of the corresponding cell fate and downregulating markers of the alternative cell fate (Desai et al., 2014; Treutlein et al., 2014). However, it is unknown how alveolar cell number, morphology and fate are regulated during subsequent lung maturation. In particular, how do AT1 cells adopt their convoluted morphology in coordination with the formation of the honeycomb-like alveolar structure? When and to what extent are the fates of AT1 and AT2 cells specified?

In this study, we focus on the poorly understood AT1 cells during the perinatal period. We develop a new marker-based stereology method to follow the change in cell number and alveolar surface area, and use single-cell three-dimensional (3D) imaging and three AT1 cell genetic drivers to follow changes in cell morphology and cell fate plasticity. We show that AT1 cells develop via a non-proliferative two-step growth process of cell flattening and cell folding, but retain cellular plasticity. Furthermore, AT1 cells, but not AT2 cells, express *Vegfa*, and disruption of AT1 cell development leads to reduced alveolar angiogenesis. These findings pave the way for future investigation of the role of AT1 cells in alveolar maturation and of AT1 cell plasticity *in vivo*.

RESULTS

AT1 cell growth fuels postnatal alveolar growth

To understand AT1 cell development, we first set out to determine the number of AT1 cells during postnatal lung growth in mice. AT1 cells have been commonly identified based on morphology using electron microscopy (Stone et al., 1992; Weibel, 2015), which limits the analysis to small regions and makes it technically challenging to obtain the total cell number as it requires the dissector method (Hsia et al., 2010) or an assumption of uniform nuclear shapes (Kauffman et al., 1974; Weibel, 2015). This prompted us to develop a new marker-based stereology method that combines stereological sampling principles with 3D imaging of molecular markers (Fig. S1A). Our method has several advantages. First, we confirmed that, unlike membrane-localized AT1 markers, HOPX stains both the nucleus and cytosol of AT1 cells (Barkauskas et al., 2013), thus allowing nucleus-based cell counting. HOPX expression was AT1 specific throughout postnatal development, as alveolar epithelial cells were marked in a mutually exclusive manner by nuclear HOPX and LAMP3 [an AT2 cell marker (Chang et al., 2013; Desai et al., 2014)] or by nuclear HOPX and cuboidal E-cadherin (E-CAD;

[1]Department of Pulmonary Medicine, The University of Texas M. D. Anderson Cancer Center, Houston, TX 77030, USA. [2]University of Puerto Rico – Medical Sciences Campus, San Juan, Puerto Rico 00927. [3]Tecnologico de Monterrey – Escuela de Medicina, Monterrey 64710, Mexico. [4]Department of Orthopedics, Kyoto University, Sakyo, Kyoto 606-8507, Japan. [5]Center for Stem Cells and Developmental Biology, The University of Texas M. D. Anderson Cancer Center, Houston, TX 77030, USA.
*These authors contributed equally to this work

‡Author for correspondence (jchen16@mdanderson.org)

Received 25 August 2015; Accepted 11 November 2015

Development (2016) 143, 54-65 doi:10.1242/dev.130005

cadherin 1) staining that colocalized with SFTPC (an AT2 cell marker) (Fig. 1A,B, Fig. S1E). Second, we developed a whole-mount thick-section staining method that minimized tissue shrinkage as well as dehydration when stained on slides (Fig. S1B,C). Third, we used 3D fluorescence imaging and Imaris software to directly visualize and count cells in large fields to reduce edge effect and bias from field selection (Fig. 1B) (Williams and Rakic, 1988). Results from this direct counting method were comparable to those using the optical dissector method (Hsia et al., 2010) (Fig. S1F). Our measurements of alveolar cell number and surface area in the adult mouse lung were in general agreement with the widely variable measurements in the literature (Fig. S1G).

Using this method, we found that as the lung continued to grow postnatally, there was a parallel increase in the number of AT2 cells, resulting in a nearly 6-fold increase in AT2 cell number from P0 to P54 (Fig. 1C, Table S1). By contrast, over the same period, the number of AT1 cells only increased ∼2-fold and most of the increase occurred within the first week after birth, possibly owing to the differentiation of remaining embryonic progenitors (Fig. S2; as described below) (Alanis et al., 2014; Yang and Chen, 2014). Such a difference was also reflected in a previously unappreciated decrease in the ratio between the numbers of AT1 and AT2 cells postnatally (Fig. 1C, Table S1). Furthermore, AT2 but not AT1 cells express the proliferative marker KI67 (Fig. S3A). Few apoptotic AT1 or AT2 cells were observed (Fig. S3B) (Schittny et al., 1998). Despite their smaller number, AT1 cells constituted nearly all the alveolar surface throughout postnatal development, as measured using STEPanizer (Fig. 1C, Table S1). Therefore, AT1 cell growth, but not proliferation, fuels most of the postnatal alveolar growth with a limited contribution from AT2 cells on a structural level.

AT1 cells flatten in conjunction with molecular specification

Next, we examined how AT1 cells grow and the relationship of this growth to postnatal alveolar maturation. The boundaries of the ultrathin cellular extensions of AT1 cells are only reliably detected by electron microscopy, which limited the analysis to two dimensions and sections capturing only part of an AT1 cell (Weibel, 1971, 2015). As a result, the complete morphology of a single AT1 cell in the developing and mature lung is unknown. To examine whole AT1 cells in 3D, we titrated down the dose of the recombination inducer (tamoxifen) to genetically label isolated cells with a membrane-bound reporter (Muzumdar et al., 2007). We also developed whole-mount multicolor staining and imaging methods to visualize labeled cells without physical sectioning and in conjunction with molecular markers (Figs 2 and 3). Multicolor reporters, such as *Rosa*^{Confetti} (Snippert et al., 2010), were not used because the soluble reporter proteins do not efficiently mark the

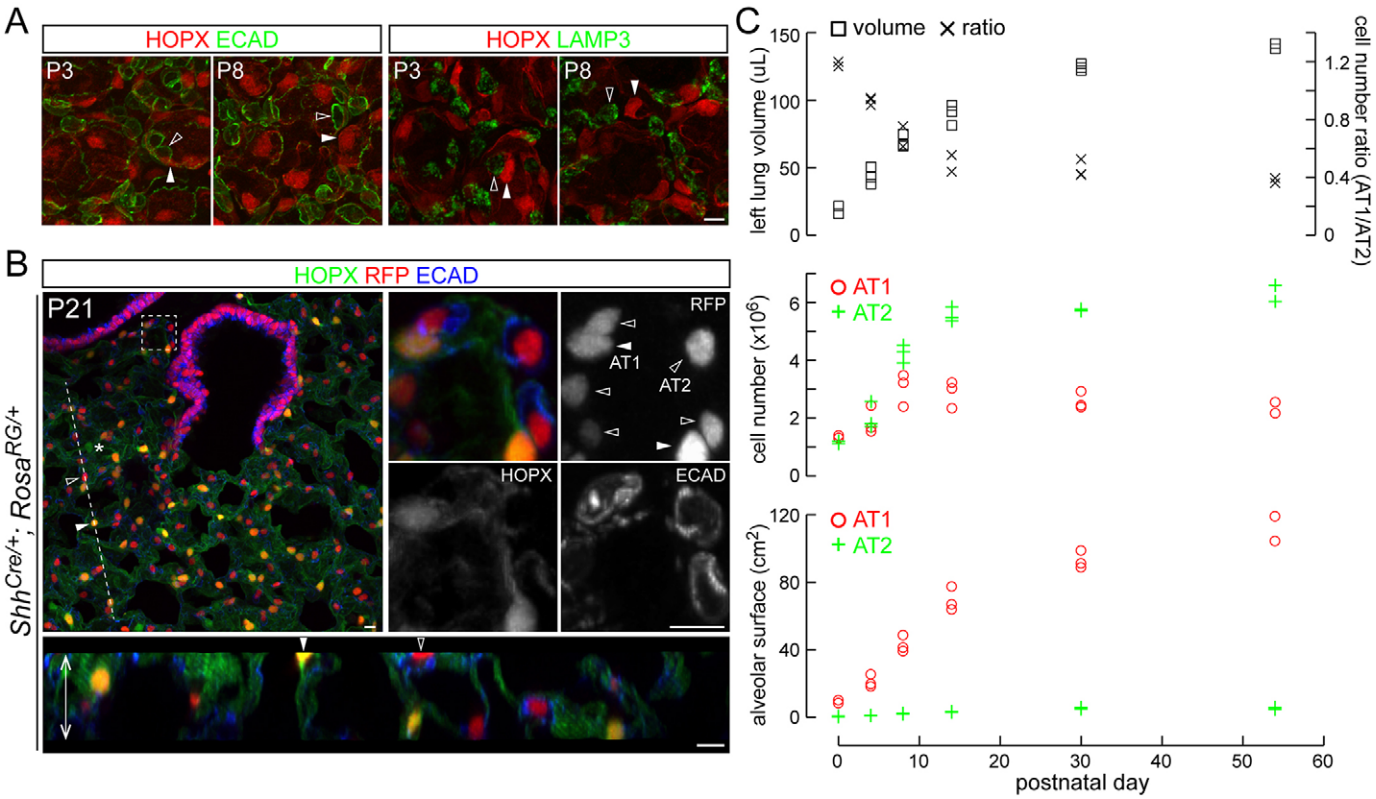

Fig. 1. AT1 cell growth fuels postnatal alveolar growth as quantified using marker-based stereology. (A) Confocal projection images of whole-mount immunostained mouse lung strips showing that HOPX (solid arrowhead) and cuboidal E-CAD or LAMP3 (open arrowhead) are mutually exclusive. Any apparent partial overlap is due to the projection view of image stacks, which allows better assignment of the staining to the corresponding nucleus. (B) Confocal projection images of a whole-mount immunostained 60 µm section from a P21 *Shh*$^{Cre/+}$; *Rosa*$^{RG/+}$ lung. Cre recombination and therefore RFP is restricted to airway and alveolar epithelial cells. Only endogenous RFP but not GFP from the *Rosa*^{RG} allele is detectable. The boxed region is enlarged in the righthand panels showing that RFP-expressing cells are marked in a mutually exclusive manner by HOPX (AT1, solid arrowhead) and E-CAD (AT2, open arrowhead). Beneath is a transverse section (z-axis) view along the dashed line showing that half AT1 (solid arrowhead) and AT2 (open arrowhead) can be discerned and counted at the image borders (double-sided arrow). Asterisk marks 'escaping' epithelial cells, presumably due to inefficient recombination or RFP expression. (C) The left lung volume, the ratio between AT1 and AT2 cell numbers, the total number of AT1 and AT2 cells, and alveolar surface area made of AT1 and AT2 cells in the left lung are plotted against animal age. Each symbol represents one mouse. Note that 1 cm^2 equals 10^8 µm^2. Scale bars: 10 µm.

Development (2016) 143, 54-65 doi:10.1242/dev.130005

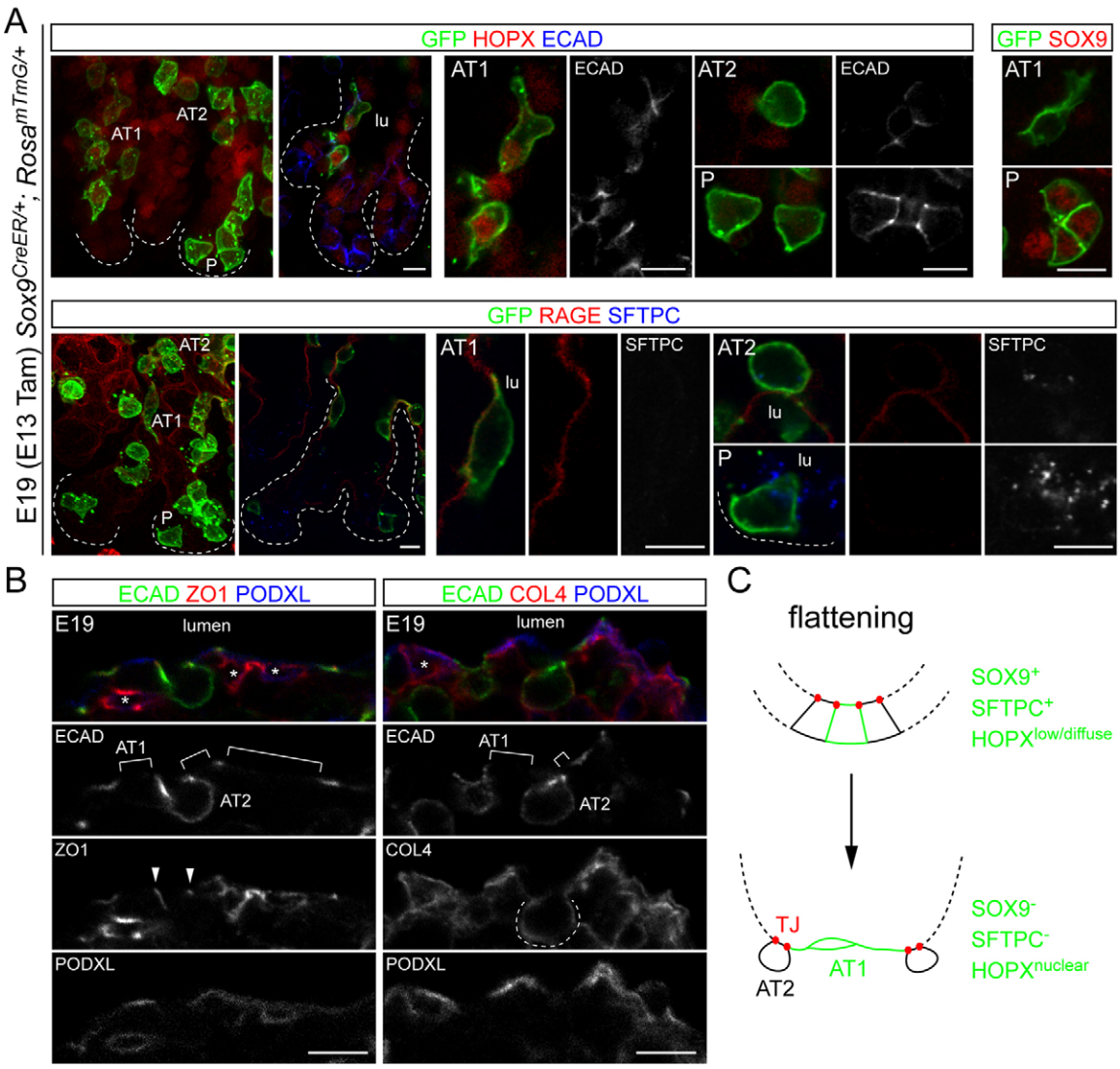

Fig. 2. AT1 cells flatten in conjunction with molecular specification. (A) Confocal images of immunostained strips from E19 *Sox9*$^{CreER/+}$; *Rosa*$^{mTmG/+}$ lungs with recombination induced at E13 (Tam, tamoxifen). The two leftmost images are maximal projection views of branch tips (dashed outlines). Columnar wedge-shaped epithelial progenitors (P) are found in branch tips. Elongated AT1 cells and cuboidal AT2 cells are found in branch stalks and also shown in section views in subsequent images with the epithelial basement membrane outlined with dashes and the lumen (lu) labeled. Only part of a cell is visible in the section view and therefore may have a different morphology from that in the projection view. Note that AT2 cells, unlike AT1 and progenitor cells, are extruded from the lumen. Elongated AT1 cells have nuclear HOPX expression and have lost progenitor and AT2 cell markers, including SOX9 and SFTPC. (B) Confocal images of E19 lung sections. PODXL-expressing AT1 cells (square bracket) are connected with neighboring AT2 cells through apically restricted tight junctions [ZO1 (TJP1), arrowheads]. E-CAD is also enriched apically at AT1-AT2 and AT1-AT1 junctions, as opposed to accumulating throughout the lateral sides between progenitors (A). Dashed line indicates epithelial basement membrane marked by collagen type IV (COL4). Asterisks mark blood vessels that express PODXL, ZO1 and COL4 but not E-CAD. (C) A model of AT1 cell flattening. As columnar wedge-shaped progenitors flatten to become AT1 cells, apical tight junctions (TJ) are maintained whereas lateral junctions are lost. Cell flattening is accompanied by changes in marker expression including SOX9, SFTPC and HOPX. Scale bars: 10 µm.

ultrathin AT1 cell extensions and because the GFP antibody, which provides the necessary signal amplification, does not distinguish GFP variants, including CFP and YFP.

To ensure unbiased analyses of the earliest stage of AT1 cell growth, we used the *Sox9*^{CreER} allele to label lung epithelial progenitors at E13, before any detectable AT1 cell differentiation (Rawlins et al., 2009; Chang et al., 2013; Alanis et al., 2014; Yang and Chen, 2014). As shown in Fig. 2A, labeled E19 lungs contained epithelial cells of three morphological types: columnar wedge-shaped cells in the most distal tube-like structure (branch tips), and a mixture of cuboidal and elongated cells in the near distal sac-like structure (transformed branch stalks, see also Fig. 4A and Fig. S4A). The columnar cells expressed SOX9, a progenitor marker (Yang and Chen, 2014), together with SFTPC and RAGE (AGER), and were therefore likely to be the bipotential progenitors (Desai et al., 2014). Consistent with this possibility, clusters of SOX9-expressing cells at the distal edge at E19 were lineage traced into both AT1 and AT2 cells in the mature lung (Fig. S2). The elongated cells were variable in morphology, ranging from leaf-shape with irregular smooth protrusions to spindle-shape with stretched sharp tips, and expressed RAGE and nuclear HOPX, consistent with them being developing AT1 cells. Although infrequent, such elongated morphology was detected as early as E17 (Fig. S4A). In comparison, the cuboidal cells expressed SFTPC but not SOX9, consistent with them being developing AT2 cells.

Development (2016) 143, 54-65 doi:10.1242/dev.130005

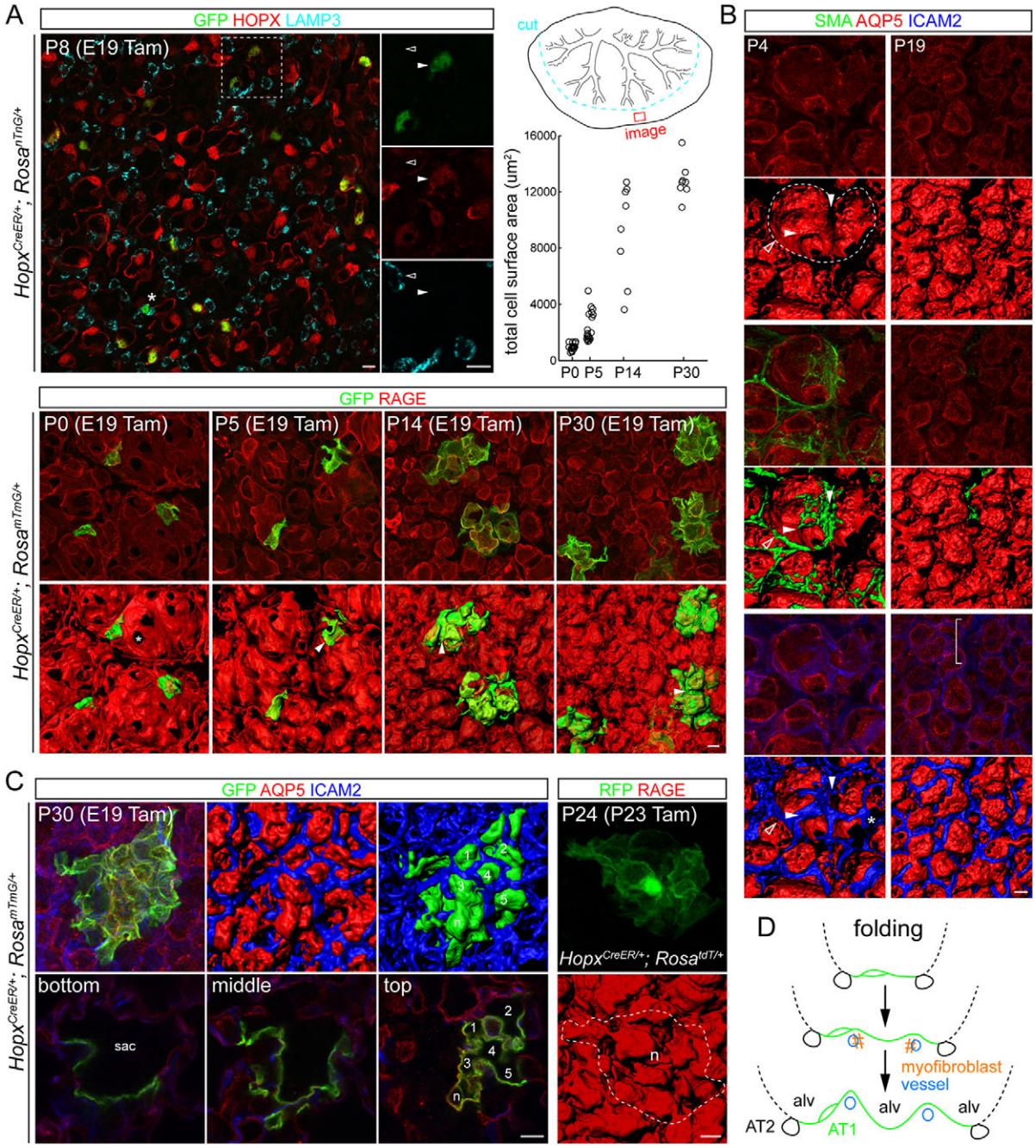

Fig. 3. AT1 cells fold in conjunction with alveolar septation. (A) (Top) Confocal projection images of immunostained strips from a P8 *Hopx*^{CreER}*; Rosa*$^{nTnG/+}$ lung showing infrequent mistargeting of AT2 cells (asterisk) by *Hopx*^{CreER} when induced with 2 mg tamoxifen at E19. Solid arrowhead, AT1 cells; open arrowhead, AT2 cells. To the right is a schematic of a cranial lobe with airways traced according to a real sample stained for SOX2 to illustrate that a strip in the gas exchange compartment is cut along the dashed line and immunostained and the boxed region imaged. The plot shows quantification of AT1 cell total surface area (both the apical and basal surface). Representative examples are shown in the bottom panels. The plot is distributed along the *x*-axis to avoid excessive overlapping. (Bottom) Confocal projection images (top row) of immunostained strips from *Hopx*^{CreER}*; Rosa*$^{mTmG/+}$ lungs at the indicated stages induced with 0.4 mg tamoxifen at E19, with the corresponding surface rendering (bottom row). Arrowheads, 'valleys' of AT1 cells; Asterisk, AT2 cell. (B) Confocal projection images of immunostained lung strips and corresponding surface rendering (beneath each confocal image). At P4 (left column), primary saccules are island-like and associated with deeper and wider grooves (dashed line, see also the P0 lung in A) with embedded smooth muscles (open arrowhead). Shallow grooves with smooth muscles begin to form on the surface of primary saccules (solid arrowheads). Vessels are associated with all grooves and only appear double layered (asterisk) between primary saccules. At P19 (right column), SMA-expressing myofibroblasts mostly disappear, whereas vessels persist to mark grooves between mature alveoli. Primary saccules are no longer obvious as secondary septa have deepened. Square brackets indicate pre-capillary arterioles surrounded by smooth muscles. (C) (Left) Projection view (top left), surface rendering (top middle and right) and section views at the indicated depth (bottom row) of confocal images of immunostained strips from a P30 *Hopx*^{CreER}*; Rosa*$^{mTmG/+}$ lung induced with 0.4 mg tamoxifen at E19. A single AT1 cell (n, nucleus) spans multiple alveoli (1 through 5, demarcated by vessels) and the underlying alveolar sac (sac). (Right) Projection view (top) and surface rendering (bottom) of confocal images of immunostained strips from a P24 *Hopx*^{CreER}*; Rosa*$^{tdT/+}$ lung induced with 0.4 mg tamoxifen at P23. The soluble reporter (RFP, pseudocolored green) highlights the nucleus of a single AT1 cell (dashed outline). (D) A model of AT1 cell folding. Flattened AT1 cells undergo a >10-fold expansion in surface area and fold where myofibroblasts temporally and vessels permanently reside. As a result, a mature AT1 cell spans multiple alveoli (alv). Scale bars: 10 µm.

Development (2016) 143, 54-65 doi:10.1242/dev.130005

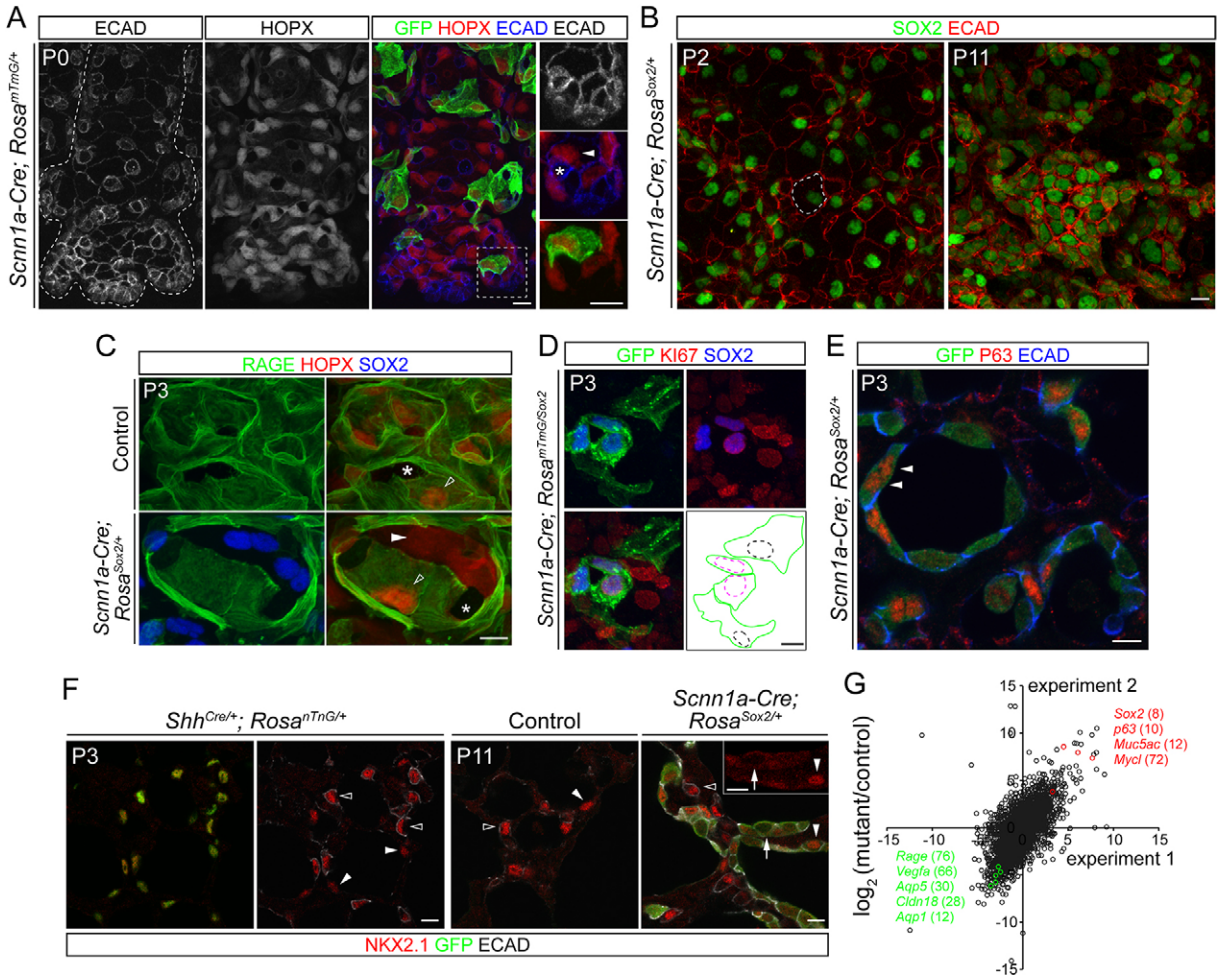

Fig. 4. *Scnn1a-Cre*-driven ectopic SOX2 expression reprograms flattened AT1 cells. (A) Confocal projection images of immunostained P0 *Scnn1a-Cre; Rosa*$^{mTmG/+}$ lung strips. Dashed lines denote a branch-like tube at the lobe edge with distal tips containing progenitors in clusters and proximal stalks containing intermingled flattened AT1 and cuboidal AT2 cells. The boxed region is enlarged to the right. Note that all labeled cells are flattened AT1 cells (demarcated by E-CAD junctions) with nuclear HOPX (arrowhead), rather than cuboidal AT2 cells (asterisk). (B) Confocal projection images of immunostained *Scnn1a-Cre; Rosa*$^{Sox2/+}$ lung strips at the indicated stages showing that isolated flattened mutant AT1 cells (demarcated by E-CAD junctions, dashed lines) form clusters with compact cell arrangement over time. (C-E) Projection (C,D) or section (E) view of confocal images of immunostained strips from littermate control (C) and *Scnn1a-Cre; Rosa*$^{Sox2/+}$ (C,E) or *Scnn1a-Cre; Rosa*$^{mTmG/Sox2}$ (D) mutant lungs. (C) Compared with AT1 cells in the control lung or neighboring unrecombined AT1 cells (open arrowhead), mutant AT1 cells (solid arrowhead) lose RAGE expression and have diffuse HOPX expression. Asterisks denote AT2 cells. (D) The *Rosa*^{mTmG} allele is easier to recombine than the *Rosa*^{Sox2} allele, generating juxtaposed GFP-labeled AT1 cells with and without SOX2 expression. Compared with control AT1 cells (green outline with black dashed nuclei), mutant AT1 cells are smaller and express the proliferation marker KI67 (green outline with red dashed nuclei). Note additional KI67 expression in mesenchymal cells. (E) Mutant AT1 cells express the basal cell marker P63 (arrowhead). (F) Left two panels show confocal images of a control lung section showing that NKX2.1 is expressed by both AT1 (solid arrowheads) and AT2 (open arrowheads, cuboidal E-CAD staining) cells. All epithelial cell nuclei are genetically marked by GFP to allow co-staining with the rabbit anti-NKX2.1 antibody. Right two panels are confocal images of sections from littermate control and *Scnn1a-Cre; Rosa*$^{Sox2/+}$ mutant lungs. Mutant AT1 cells marked by GFP have nuclear (solid arrowhead) or diffuse (arrow) NKX2.1. Inset shows NKX2.1 single-channel image. NKX2.1 expression in AT2 cells (open arrowhead, cuboidal E-CAD staining) of the mutant lung is not affected. (G) Scatterplot of $\log_2$ fold change in gene expression between two biological replicates. Compared with littermate control (*Scnn1a-Cre; Rosa*$^{mTmG/+}$) AT1 cells, mutant (*Scnn1a-Cre; Rosa*$^{Sox2/+}$) AT1 cells downregulate AT1 markers (green) and upregulate airway markers (red). The number in parenthesis denotes the rank order in fold change among genes that are significantly different between control and mutant. Scale bars: 10 µm.

Throughout such changes in cell morphology, the elongated cells remained connected to their cuboidal neighbors via apically restricted tight junctions and apically enriched adherens junctions (Fig. 2B). Interestingly, the basolateral side of the cuboidal cells contained E-CAD and was surrounded by a continuous basement membrane instead of adjacent AT1 cells (Fig. 2B). Such apically restricted contact between AT1 and AT2 cells positioned AT2 cells in the interstitial region rather than the lumenal space (Fig. 2B), an arrangement also observed for AT2 cells labeled individually (Fig. 2A) and at later postnatal stages (Fig. S5). These results suggested that, in the initial step of AT1 cell growth, columnar wedge-shaped progenitors flatten while maintaining apical tight junctions but losing lateral adherens junctions, a process accompanied by cell type-specific molecular changes (Fig. 2C).

AT1 cells fold in conjunction with alveolar septation

To specifically label AT1 cells and follow their subsequent growth, we screened seven *Cre* and *CreER* alleles of genes that were expected to be active in the lung epithelium and therefore potentially in AT1 cells. We characterized all of the alleles throughout embryonic and postnatal stages using the same Cre reporter

Development (2016) 143, 54-65 doi:10.1242/dev.130005

Rosa^{mTmG} to allow direct comparison. Whereas some alleles had a very low (*Krt8-CreER*, *Krt18-CreER*, *Krt14-Cre*, *Cldn6*^{CreER}) or non-selective (*Nkx2.1*^{CreER}) activity in the lung epithelium, *Scnn1a-Cre* (described below) and *Hopx*^{CreER} were found to be highly selective for AT1 cells (Fig. S6). When recombination was induced before E15, very rare cells were labeled by *Hopx*^{CreER} in the lung (Fig. S6F). When induced at E18, *Hopx*^{CreER} labeled elongated cells with irregular extensions, similar to the aforementioned developing AT1 cells labeled by *Sox9*^{CreER} (Fig. S4B). Although *Hopx*^{CreER} can label AT2 cells (Jain et al., 2015), such leaky targeting was infrequent when induced at E19 using the nuclear reporter *Rosa*^{nTnG} (Prigge et al., 2013) (7/189 GFP^{+} cells from three mice; Fig. 3A), suggesting that *Hopx*^{CreER} has limited activity in bipotential progenitors. Labeled AT1 cells were readily identified by their characteristic thin cellular extensions that were marked by *Rosa*^{mTmG} (Fig. 3, Fig. S6F).

Timecourse morphological analysis using *Hopx*^{CreER} revealed that AT1 cells underwent a folding process, whereby the initial flattened cells were sculptured into 'mountains' and 'valleys' (Fig. 3A). Although individually variable at a given time point, AT1 cells, as a population, had an increase in total cell surface area of more than 10-fold and reached a maximum of ~12,000 µm^2 by P30 (Fig. 3A). The total (apical and basal) surface area of individual cells was comparable to the average apical surface area calculated from the stereology data (Table S1) and the literature (Stone et al., 1992), with the difference attributed to tissue shrinkage (Fig. S1C) and possibly preferential labeling of AT1 cells that are more mature by *Hopx*^{CreER} at a limiting dose of tamoxifen.

Notably, AT1 cell folding became apparent from P5, which coincided with transformation of the smooth-walled primary alveolar saccules into the honeycomb-like mature alveoli (Fig. 3A), a process known as secondary septation (Herzog et al., 2008). To further investigate this, we developed whole-mount staining methods to visualize the septation in 3D. At P4, grooves of various orientation and depth were visible on the alveolar surface subdividing the primary alveolar saccules (Fig. 3A,B). Most grooves contained smooth muscle actin-expressing cells, consistent with them being the myofibroblast-associated secondary septa (Herzog et al., 2008). All the grooves matched a network of vessels, which persisted even after the myofibroblasts disappeared after P19 (Fig. 3B). Therefore, compared with the transient nature of the myofibroblasts, the vessels are a more consistent and permanent marker of secondary septa. The apparent similarity in the size of the alveolar pocket between P4 and P19 is likely to be due to the formation of secondary septation, despite the increase in total alveolar surface area by 3- to 4-fold (Table S1). Interestingly, unlike the capillary maturation model (Burri, 1984), all vessels were parallel, instead of perpendicular, to the grooves and therefore did not bend to form a hairpin-like double-layered structure inside the grooves. Double-layered vessels were only observed at the interface between adjacent primary alveolar saccules where the vessel networks associated with individual saccules were juxtaposed (Fig. 3B).

Co-staining of individual folded AT1 cells with vessels revealed that the 'valleys' of AT1 cells matched the vessels and thus were considered to result from secondary septation, while the 'mountains' corresponded to alveoli from subdivided primary saccules (Fig. 3). As a result of cell folding, a single AT1 cell could span multiple alveoli and reach the more centrally located alveolar sac (Fig. 3C, see Fig. 3A for additional examples). Similar cell morphology was observed using the soluble reporter *Rosa*^{tdT} (Madisen et al., 2010), which also highlighted the nucleus, thus confirming that our approach labeled individual cells (Fig. 3C). These data suggest that AT1 cells further expand via a folding process that matches the formation of capillaries and secondary septa (Fig. 3D).

Developing AT1 cells retain cellular plasticity

Having shown that AT1 cells grow via a non-proliferative two-step process, we sought to determine when and to what extent AT1 cells were committed to this growth process. Since little is known about the genes controlling AT1 cell development, we tested whether AT1 cells could change their fate upon ectopic expression of SOX2, a transcription factor that is normally restricted to the airways and promotes airway differentiation (Gontan et al., 2008; Que et al., 2009; Tompkins et al., 2009, 2011; Alanis et al., 2014). We first used the *Scnn1a-Cre* allele identified in our driver screen that targeted AT1 cells in the flattening stage and were thus committed to terminal differentiation. Although SCNN1A was detected in other cell types than AT1 (Borok et al., 2006; Johnson et al., 2002, 2006; Kimura et al., 2011), the *Scnn1a-Cre* allele was active in AT1 cells after E19, consistent with the perinatal upregulation of *Scnn1a* in the distal lung epithelium (Fig. S7D) (Chang et al., 2013), and reached a targeting efficiency (defined as the percentage of AT1 cells that were targeted) of 71% (n=153 cells) and specificity (defined as the percentage of targeted cells that were AT1 cells) of 95% (n=176 cells from three mice) (Fig. 4A, Fig. S7). As expected from this AT1 cell specificity, SOX2-expressing cells in the *Scnn1a-Cre; Rosa*$^{Sox2/+}$ lung initially had isolated nuclei and the flattened morphology that was demarcated by E-CAD junctions (P2 in Fig. 4B). Strikingly, at P11, mutant cells formed large clusters with a compact cell arrangement reminiscent of that of the airways (Fig. 4B). Mutant cell clusters remained largely monolayered surrounding the airspace and thus appeared less dramatic in section views (e.g. Fig. 4F).

Compared with control lungs or adjacent normal AT1 cells in the same lung, targeted AT1 cells maintained a normal level, albeit diffuse pattern, of HOPX expression, but downregulated other AT1 cell markers including RAGE, upregulated the proliferation marker KI67 (26% of n=191 cells at P11; none in control AT1 cells; three mice in each group), and expressed an isoform of P63 (TRP63) specific for basal cells (52% of n=305 cells at P11; none in control AT1 cells; three mice in each group) (Fig. 4C-E, Fig. S8A). However, only occasional mutant AT1 cells expressed additional basal or other airway cell markers, including KRT5, KRT14 and CCSP (SCGB1A1) (Fig. S8A), suggesting that the high level of SOX2 expression from the *Rosa*^{Sox2} allele did not support physiological airway differentiation. In contrast to prior reports (Ikeda et al., 1995; Zhou et al., 1996), NKX2.1, a lung lineage transcription factor, was expressed by both AT1 and AT2 cells, and frequently lost its nuclear localization in mutant AT1 cells (Fig. 4F). This was associated with upregulation of MUC5AC (Fig. 4G, Fig. S8A), reminiscent of the gene expression changes associated with the formation of mucinous adenocarcinomas upon loss of NKX2.1 (Winslow et al., 2011; Maeda et al., 2012; Snyder et al., 2013). These gene expression changes were confirmed by transcriptome profiling of FACS-purified control and mutant AT1 cells, which identified additional SOX2-suppressed AT1 cell markers (Fig. 4G, Fig. S9, Table S2).

Although *Scnn1a-Cre* targeted occasional AT2 cells, such leaky targeting (5%) could not account for the high percentage of mutant AT1 cells expressing KI67 (26%) and P63 (52%) and the robust clustering of mutant cells (Fig. 4B). To further substantiate the observed AT1 cell plasticity, we activated *Rosa*^{Sox2} with an independent *Cre* allele, *Aqp5*^{Cre} (Flodby et al., 2010), which

Development (2016) 143, 54-65 doi:10.1242/dev.130005

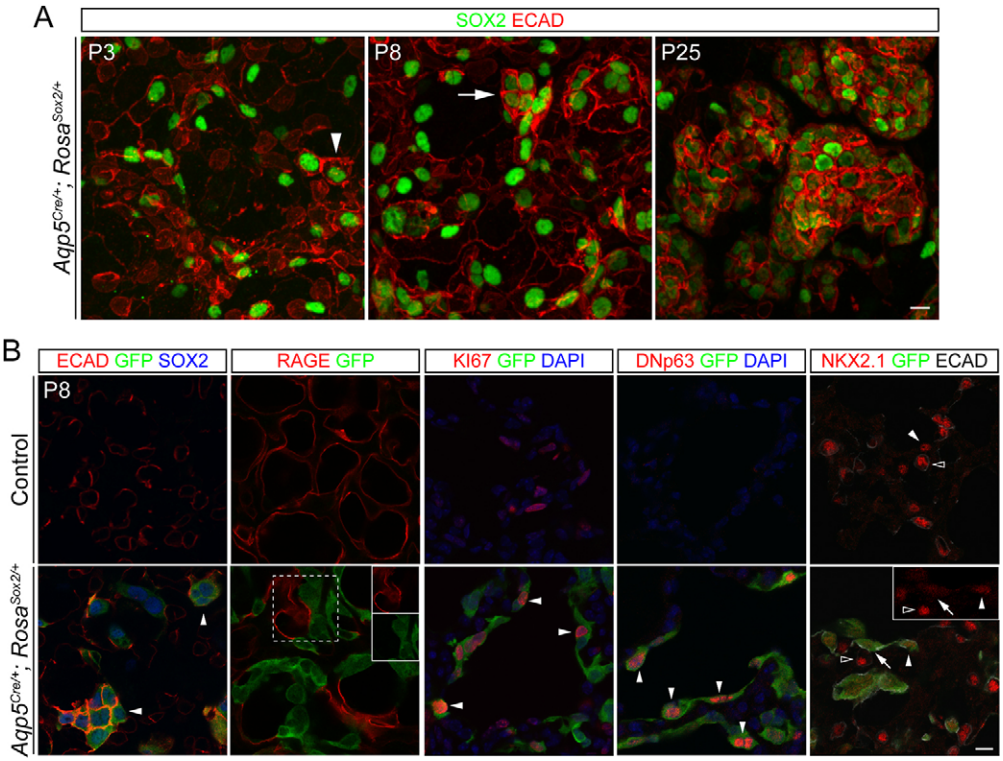

Fig. 5. *Aqp5*^{Cre}-driven ectopic SOX2 expression reprograms flattened AT1 cells. (A) Confocal projection images of immunostained *Aqp5*$^{Cre/+}$; *Rosa*$^{Sox2/+}$ lung strips at the indicated stages. Some mutant AT1 cells (arrowhead) have retracted their cellular extensions and accumulate a high level of E-CAD at P3. Mutant cell clusters (arrow) are present at P8. (B) Confocal images of sections from littermate control and mutant lungs showing comparable phenotypes of AT1 cells targeted with *Aqp5*^{Cre} to those targeted with *Scnn1a-Cre* (Fig. 4). Mutant AT1 cells (GFP, arrowhead) form clusters, downregulate RAGE (boxed region shown as single-channel images in insets), express KI67 and DNp63 (deltaNp63), and have diffuse (arrow) or nuclear (solid arrowhead) NKX2.1 (single-channel image shown in inset). NKX2.1 expression in AT2 cells (open arrowhead, cuboidal E-CAD staining) of the mutant lung is not affected. KI67 is expressed in non-AT1 cells in the control lung (Fig. S3A). Scale bars: 10 µm.

targeted AT1 cells with an efficiency of 89% (n=329 cells) and a specificity of 99% (n=317 cells from three mice) (Fig. S7). Essentially the same phenotypes were observed, including cluster formation over time (Fig. 5A), cell proliferation (KI67, 39% of n=161 cells at P8; none in control AT1 cells; three mice in each group), downregulation of AT1 markers and upregulation of airway markers (P63, 42% of n=146 cells at P8; none in control AT1 cells; three mice in each group) (Fig. 5B, Fig. S8A). SOX2-induced P63 expression was specific to AT1 cells, as *Rosa*^{Sox2} activation in airway cells by *Sox2*^{CreER} (Alanis et al., 2014) or in mesenchymal cells by *Tbx4-Cre* (Kumar et al., 2014) did not lead to ectopic P63 expression (Fig. S8B,C). Therefore, the overexpression of a single gene is sufficient to reprogram flattened AT1 cells toward the airway cell fate and allow them to proliferate.

AT1 cells are the source of *Vegfa*

Interestingly, the angiogenic factor *Vegfa* was downregulated by 16-fold in SOX2-expressing mutant AT1 cells (Fig. 4G, Table S2), an unexpected change given previous evidence for AT2 cells being the source of *Vegfa* (Bhatt et al., 2001; Ng et al., 2001). To pinpoint the cellular source of *Vegfa*, we developed a combined fluorescence *in situ* hybridization and immunostaining protocol and found that the perinuclear localization of the *Vegfa* mRNA allowed assignment of its expression to AT1 cells, but not AT2 cells (Fig. 6A), consistent with a recent single-cell transcriptome analysis (Treutlein et al., 2014). *Vegfa* mRNA was present in the alveolar epithelium at E18 and at a lower level in the distal progenitors (Fig. 6A). Notably, *Vegfa* expression was lost in SOX2-expressing mutant AT1 cells, whereas the AT2 cell marker *Sftpc* was not affected (Fig. 6B,C). This was accompanied by a simplified vascular network, as determined using the endothelial marker ICAM2, which labels both cell junctions and cell surface (Halai et al., 2014), and a lower, albeit variable, density of endothelial cells as determined using the endothelial nuclear marker ERG (Birdsey et al., 2015) (three mice in each group; Fig. 6C). These results suggested that normal AT1 cell development is required for alveolar angiogenesis.

Mature AT1 cells retain cellular plasticity

Lastly, we examined the plasticity of mature AT1 cells by activating *Rosa*^{Sox2} with the inducible *Hopx*^{CreER} allele. *Hopx*^{CreER}-induced recombination was almost exclusive to AT1 cells after 5 weeks, with an efficiency of 21% and specificity of 98% (n=248 cells from three mice) using *Rosa*^{mTmG} (Fig. 7A). When *Rosa*^{Sox2} was activated at least 5 weeks after birth in AT1 cells that had completed the folding process, mutant AT1 cells fully retracted their cellular extensions within 21 days and therefore were much smaller than their normal counterparts (Fig. 7A). This difference was better demonstrated when comparing control and mutant AT1 cells in the same lung, taking advantage of the lower recombination efficiency of the *Rosa*^{Sox2} allele compared with the *Rosa*^{mTmG} allele (Fig. S10A).

Although a subset of mutant AT1 cells (11%, n=72 cells from three mice) expressed KI67 at a given time (Fig. S10B), over time the majority of targeted AT1 cells formed doublets (33%) or clusters (53%; n=73 from three mice) (Fig. 7B). Owing to the low efficiency of *Hopx*^{CreER} in recombining the *Rosa*^{Sox2} allele, individual mutant doublets or clusters were isolated from each other (Fig. 7B,C) and thus were considered to originate from a single targeted AT1 cell. All mutant cells, including singlets, accumulated a high level of E-CAD (Fig. 7B). Most mutant AT1 cells, including singlets (81%, n=43 cells from three mice), activated the cell cycle gene *Ccnd1*, a putative direct target of SOX2 (Chen et al., 2008) (Fig. 7C, Fig. S10C). Such activation occurred 9 days after recombination, when mutant cells still had a single nucleus and elaborate cellular extensions and began to accumulate excessive E-CAD (Fig. 7C). Although NKX2.1 became diffuse, AT1 cell markers were maintained and no airway markers, such as P63, CCSP, FOXJ1 and MUC5AC, were observed in mutant AT1 cells (Fig. S10A,D). Therefore, compared with those in the flattening stage, AT1 cells

Development (2016) 143, 54-65 doi:10.1242/dev.130005

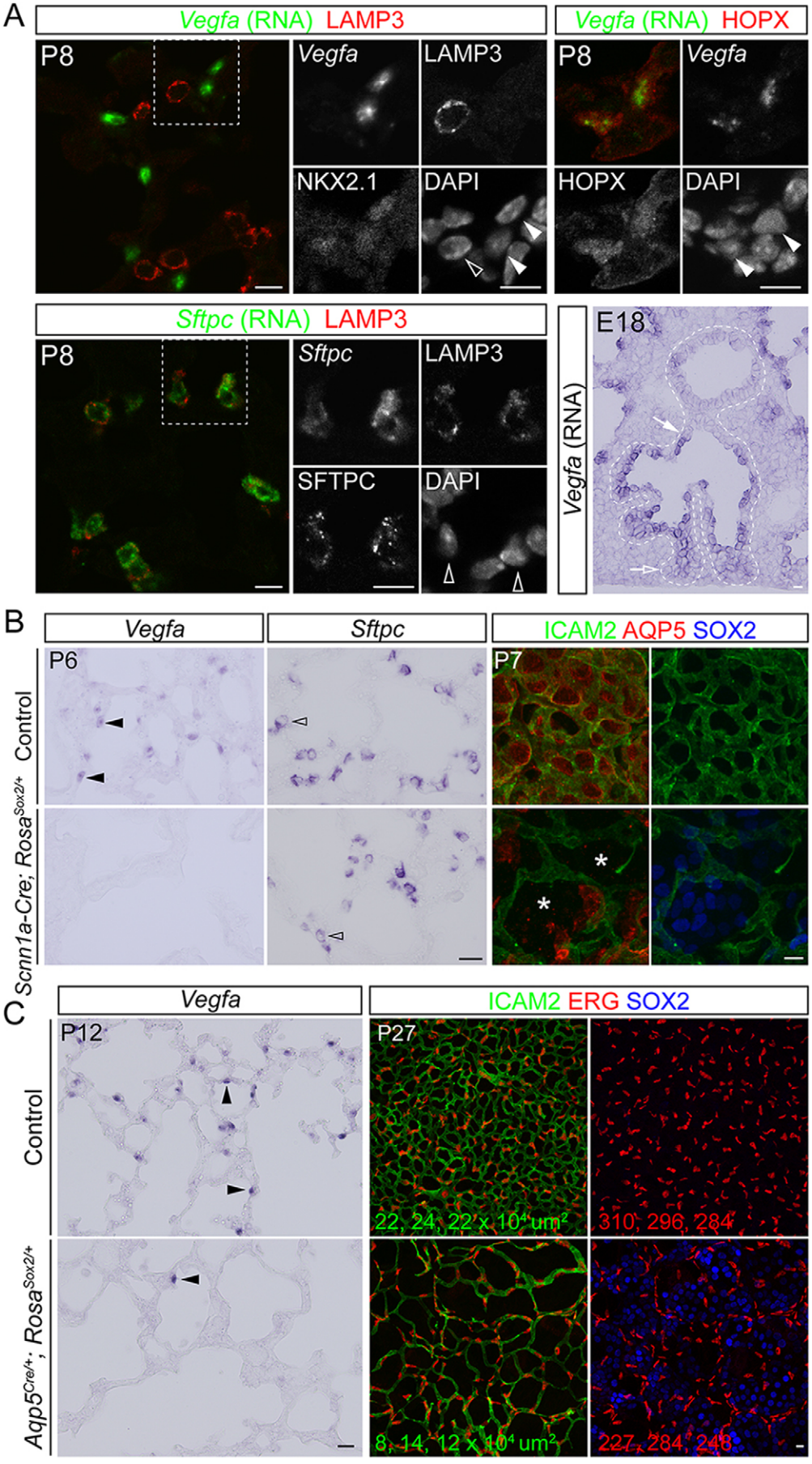

Fig. 6. AT1 cells are the source of *Vegfa*. (A) Combined fluorescence *in situ* hybridization and immunostaining of wild-type lung sections. (Top) *Vegfa* RNA localizes to oval-shaped AT1 cell bodies that are positive for NKX2.1 and HOPX (solid arrowheads), but not to LAMP3-positive cuboidal AT2 cells (open arrowhead). (Bottom) The left panel shows, as a technical control, that *Sftpc* RNA localizes to cuboidal AT2 cells that are positive for SFTPC and LAMP3. Boxed regions are enlarged in subsequent panels. To the right is a colorimetric *in situ* hybridization of an E18 lung section near the tissue edge showing *Vegfa* RNA in the alveolar epithelium (arrow, bronchoalveolar duct junction) and, at a lower level, the distal progenitors (open arrow). The epithelium is traced with a dashed line. (B) Section colorimetric *in situ* hybridization (left two columns) and confocal projection images of immunostained strips (right two columns) from littermate control and *Scnn1a-Cre; Rosa*$^{Sox2/+}$ lungs at the indicated stages. *Vegfa* expression (solid arrowheads) is lost in mutant AT1 cells, whereas *Sftpc* expression (open arrowheads) is not affected. Asterisks indicate regions with fewer vessels in the mutant. (C) Section colorimetric *in situ* hybridization (left) and confocal projection images of immunostained strips (right two columns) from littermate control and *Aqp5*$^{Cre/+}$*; Rosa*$^{Sox2/+}$ lungs at the indicated stages. The numbers indicate the vessel areas (P=0.02, Student's t-test) and the number of endothelial cells (P=0.1, Student's t-test) for three image fields of 318×318×20 µm. Scale bars: 10 µm.

Development (2016) 143, 54-65 doi:10.1242/dev.130005

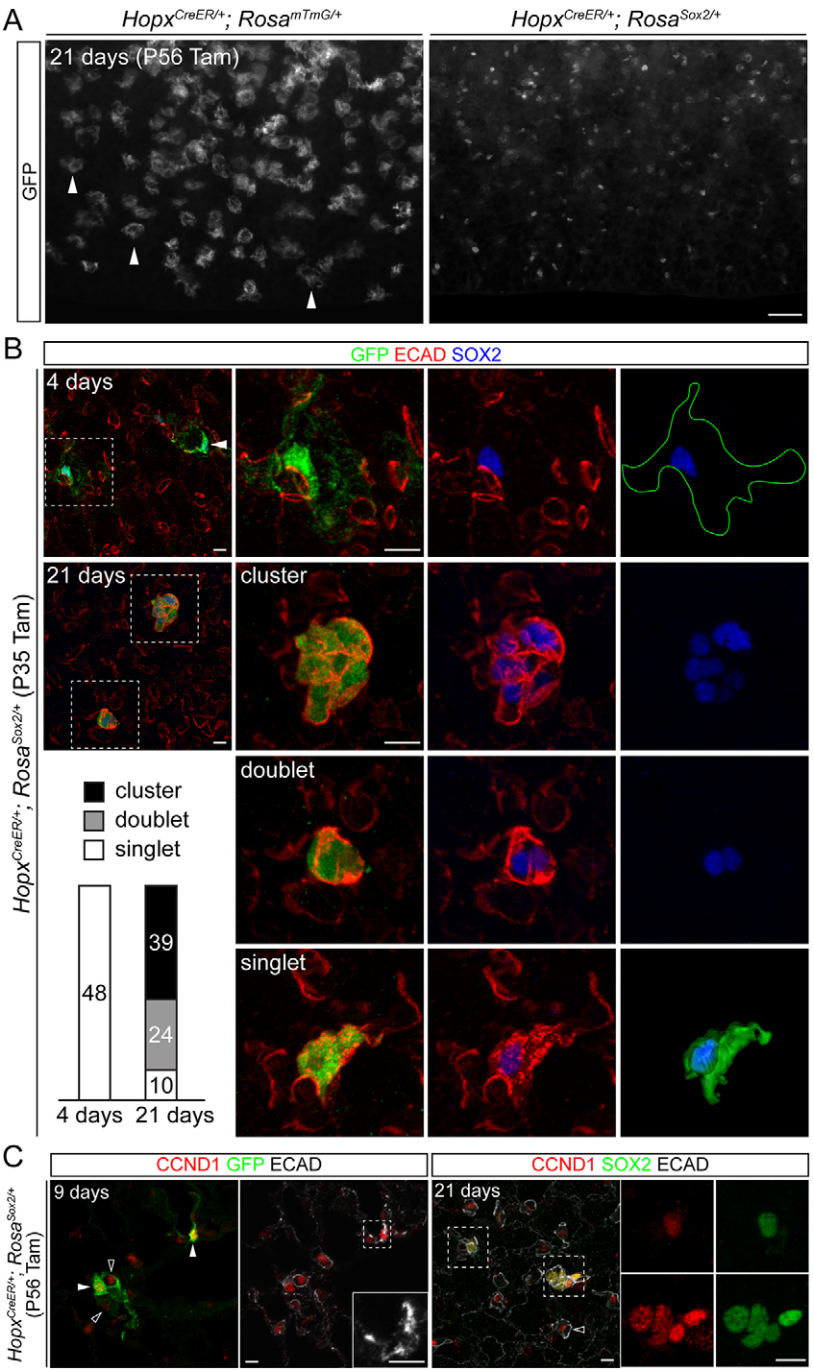

Fig. 7. Mature AT1 cells retain cellular plasticity. (A) Stereomicroscopy images of lung strips 21 days after recombination induced at P56 showing a robust response of individual AT1 cells (arrowheads) to ectopic SOX2 expression by retracting their cellular extensions. Different doses of tamoxifen were used to achieve comparable recombination efficiency of the $Rosa^{mTmG}$ (0.4 mg) and $Rosa^{Sox2}$ (4 mg daily for three consecutive days) alleles. (B) Confocal projection images of immunostained lung strips at the indicated days after recombination induced at P35. Boxed regions are enlarged in subsequent panels showing that mutant AT1 cells lose extended morphology (green outline at 4 days; arrowhead indicates another mutant cell) and form clusters, doublets or singlets (21 days). The total numbers of each type examined are shown in the bar chart. All singlets examined at 4 days after recombination have extended morphology, indicating their AT1 cell identity. Mutant AT1 cells including singlets have retracted their cellular extensions (surface rendering shown) and accumulate a high level of E-CAD. (C) Confocal images of immunostained lung sections at 9 or 21 days after recombination induced at P56. Boxed regions are shown as single-channel images. Whereas control AT1 cells do not express CCND1 (Fig. S10C), mutant AT1 cells activate CCND1 when they are still singlets (solid arrowhead), retracting their cellular extensions and starting to accumulate E-CAD (punctate staining in inset). Open arrowhead, CCND1-expressing AT2 cells. Scale bars: 100 µm in A; 10 µm in B,C.

after the folding process are less plastic in cell fate, but a majority of them (86%, doublets and clusters) retain some degree of proliferative potential.

DISCUSSION

Our results support a model of AT1 cell development whereby AT1 cells normally undergo terminal differentiation via a non-proliferative two-step process—cell flattening and cell folding. However, during and even after this process, AT1 cells maintain proliferative potential and can undergo developmental stage-dependent cell reprogramming (Fig. S11). These results demonstrate *in vivo* the plasticity of a majority of AT1 cells that had previously been suggested in isolated cells *in vitro* (Williams, 2003; Gonzalez et al., 2009). Such plasticity is consistent with a recent study showing that, at a low frequency, AT1 cells may convert to AT2 cells and proliferate upon pneumonectomy or oncogenic *Kras* expression (Jain et al., 2015). Additional work is necessary to understand whether and how AT1 cells retract their cellular extensions when converting to AT2 cells. In addition, our study has identified a list of genes suppressed by SOX2 expression (Table S2) that may control the convoluted morphology of AT1 cells or serve as signaling molecules (e.g. VEGFA) underlying the physical association between AT1 cells and endothelial cells and myofibroblasts.

This study provides insights into the cell biology of perinatal lung cell maturation, a process that is disrupted in premature birth, as well as new imaging and genetic tools for the further study of this process. Given that AT1 cells constitute >95% of the alveolar

Development (2016) 143, 54-65 doi:10.1242/dev.130005

surface area, the cellular changes of AT1 cells are expected to reflect how the tubular epithelium generated by branching morphogenesis is transformed into a honeycomb-like alveolar epithelium during the saccular and alveolar stages of lung development (Yang and Chen, 2014). According to our single-cell morphology analyses, the first flattening step increases epithelial surface to facilitate saccule formation while maintaining an interconnected epithelial sheet. Flattening of AT1 cells initiates behind the SOX9-positive branch tips, at a location where saccules first appear (Chang et al., 2013; Desai et al., 2014). After flattening, individual AT1 cells increase surface area by more than 10-fold and undergo a folding step that matches with the formation of the honeycomb-like mature alveoli, resulting in a single AT1 cell spanning multiple alveoli.

Our multicolor 3D imaging of intact alveolar tissues suggests that, besides myofibroblasts and vessels, AT1 cells are an integral component and a potential regulator of secondary septation. On sections, secondary septation appears as club-like inward growth of the saccule wall, which in 3D corresponds to grooves running in different directions along the saccule surface made of a single folded AT1 cell. On sections, the septal tips often contain smooth muscle actin-expressing myofibroblasts, which in 3D correspond to fibrous smooth muscle bundles embedded in the aforementioned grooves. Conceivably, these smooth muscle bundles might function as a 'belt' to limit structural changes locally while the rest of the saccule wall expands as the lung grows in volume. If true, the septa might not in fact grow inward but only appear to do so as the result of the relative outgrowth of the non-septa regions. Vessels are associated with the grooves as early as myofibroblasts and remain associated after the myofibroblasts disappear. This raises the intriguing possibility that septa formation might be driven and/or stabilized by vessels, while myofibroblasts might be required to overcome greater tissue mechanical resistance during septa initiation. Notably, as judged by 3D analysis, all vessels run in parallel, instead of perpendicular, to the grooves. We do not observe the double capillaries that have previously been suggested to form via hairpin-like bending of single capillaries into the septa (Burri, 1984). Further studies are necessary to test whether the previously reported double capillaries are juxtaposed vessels that are associated with two primary saccules (Fig. 3B). Given the coordination among AT1 cells, myofibroblasts and vessels, it is tempting to speculate that AT1 cells might play a signaling role in addition to their structural role during secondary septation. Indeed, our results show that AT1 cells, instead of AT2 cells, are the source of the key alveolar angiogenic factor VEGFA (Kasahara et al., 2000; Stenmark and Abman, 2005). Future genetic experiments should reveal whether AT1 cells signal to the endothelial cells by secreting angiogenic factors, such as VEGFA, and/or by forming permissive matrix substrates.

Although AT1 cells are traditionally viewed as terminally differentiated (Williams, 2003), our study shows that, at a high frequency, flattened AT1 cells undergoing terminal differentiation can be reprogrammed toward the airway fate and proliferate, and that fully differentiated AT1 cells can retract their elaborate cellular extensions and proliferate. As AT1 cells require the overexpression of a single gene to activate proliferation, it is tempting to speculate that AT1 cells might also serve a stem cell function or as the cell-of-origin for a subset of lung cancers, both of which have been shown for AT2 cells (Barkauskas et al., 2013; Desai et al., 2014). Given the substantial difference between AT1 and AT2 cells, the corresponding tumors may have distinct molecular signatures and genetic alterations. A deeper understanding of the tumorigenic potential of AT1 cells, as well as of the mechanisms normally restricting their proliferation, might implicate AT1 cells as a new cellular source for lung repair and lung cancer.

MATERIALS AND METHODS

Mice

The following mouse (*Mus musculus*) strains were used: $Rosa^{mTmG}$ (Muzumdar et al., 2007), $Rosa^{RG}$ (Shioi et al., 2011), $Rosa^{nTnG}$ (Prigge et al., 2013), $Rosa^{Sox2}$ (Lu et al., 2010), $Rosa^{tdT}$ (Madisen et al., 2010), Shh^{Cre} (Harfe et al., 2004), $Hopx^{CreER}$ (Takeda et al., 2011), $Sox2^{CreER}$ (Arnold et al., 2011), $Sox9^{CreER}$ (Soeda et al., 2010), *Scnn1a-Cre* (JAX stock number 009613), *Tbx4-Cre* (Kumar et al., 2014), $Aqp5^{Cre}$ (Flodby et al., 2010), *Krt8-CreER* (Van Keymeulen et al., 2011), *Krt18-CreER* (Van Keymeulen et al., 2009), *Krt14-Cre* (Dassule et al., 2000), $Cldn6^{CreER}$ (Anderson et al., 2008) and $Nkx2.1^{CreER}$ (Taniguchi et al., 2011). The amount of tamoxifen to achieve the desired level of recombination was determined empirically, as detailed in the supplementary Materials and Methods.

Marker-based stereology

Lungs were inflation fixed at 25 cm H_2O pressure with 0.5% paraformaldehyde (P6148, Sigma) in phosphate-buffered saline (PBS, pH 7.4). The left lobes were cryosectioned exhaustively at 60 µm with one in every 15 sections collected for whole-mount immunostaining. STEPanizer (Tschanz et al., 2011) was used to obtain lung volume and alveolar surface area. The number of AT1 and AT2 cells in the entire stack (N_v) was directly counted using Imaris (Bitplane). See the supplementary Materials and Methods for details.

Whole-mount and section immunostaining

Immunostaining was performed following published protocols (Chang et al., 2013; Alanis et al., 2014). Cell and tissue surface rendering was generated in Imaris with default settings: smoothing with surface area detail level at 0.621 µm and thresholding by local contrast at 2.33 µm. For further details, including the antibodies used, see the supplementary Materials and Methods.

Fluorescence and colorimetric *in situ* hybridization

Colorimetric section *in situ* hybridization was carried out following published protocols (Chang et al., 2013; Alanis et al., 2014). For fluorescence *in situ* hybridization, sections were incubated with 0.05 µg/ml riboprobes and a fluorescein tyramide signal amplification system (PerkinElmer, NEL741001KT) was used to detect the hybridized riboprobes. See the supplementary Materials and Methods for details.

Transcriptome profiling of FACS-purified AT1 cells

Cell dissociation and purification were performed based on a previous protocol with modifications as detailed in the supplementary Materials and Methods (Chang et al., 2013). RNA was extracted from at least 10^5 purified cells using Trizol reagents (Invitrogen, 15596018) and an RNeasy Micro Kit (Qiagen, 74004). RNAseq libraries were prepared using an mRNA isolation kit (New England BioLabs, E7490) and a NEBNext Ultra RNA Library Prep Kit (New England BioLabs, E7530S) and were sequenced on an Illumina HiSeq2000. Approximately 35-80 million 76 nt pair-end reads were generated for each sample and analyzed using standard tophat2, bowtie2 and cufflinks modules in R. The raw data were deposited in GEO under accession number GSE73861.

Acknowledgements

We thank Drs Brigid Hogan and Mark Onaitis for the $Rosa^{Sox2}$ mice; Drs Zea Borok, Edward Crandall and Per Flodby for the $Aqp5^{Cre}$ mice; Dr Samuel Ho for the MUC5AC antibody; and Dr Barry Stripp for the CCSP antibody.

Competing interests

The authors declare no competing or financial interests.

Author contributions

J.Y., B.J.H., D.M.A. and J.C. designed research; J.Y., B.J.H., D.M.A., O.N., L.V.-E. and E.J.O. performed research; E.J.O. analyzed the transcriptome data; H.A. provided the $Sox9^{CreER}$ mice; S.E.E. provided mice; J.C. and E.J.O. wrote the paper; all authors read and approved the paper.

Funding
The University of Texas MD Anderson Cancer Center DNA Analysis Facility and Flow Cytometry and Cellular Imaging Core Facility are supported by the Cancer Center Support Grant [CA #16672] from the National Institutes of Health. This work was supported by the University of Texas System Rising STARS Award, the March of Dimes Basil O'Connor Starter Scholar Research Award, the University Cancer Foundation via the Institutional Research Grant program at the University of Texas MD Anderson Cancer Center and the University of Texas MD Anderson Cancer Center Start-up Fund (J.C.) and the National Institutes of Health [R01 HL117976 to S.E.E.]. J.C. is an R. Lee Clark Fellow of The University of Texas MD Anderson Cancer Center. Deposited in PMC for release after 12 months.

Supplementary information
Supplementary information available online at
http://dev.biologists.org/lookup/suppl/doi:10.1242/dev.130005/-/DC1

References

Alanis, D. M., Chang, D. R., Akiyama, H., Krasnow, M. A. and Chen, J. (2014). Two nested developmental waves demarcate a compartment boundary in the mouse lung. *Nat. Commun.* **5**, 3923.
Anderson, W. J., Zhou, Q., Alcalde, V., Kaneko, O. F., Blank, L. J., Sherwood, R. I., Guseh, J. S., Rajagopal, J. and Melton, D. A. (2008). Genetic targeting of the endoderm with claudin-6CreER. *Dev. Dyn.* **237**, 504-512.
Arnold, K., Sarkar, A., Yram, M. A., Polo, J. M., Bronson, R., Sengupta, S., Seandel, M., Geijsen, N. and Hochedlinger, K. (2011). Sox2(+) adult stem and progenitor cells are important for tissue regeneration and survival of mice. *Cell Stem Cell* **9**, 317-329.
Barkauskas, C. E., Cronce, M. J., Rackley, C. R., Bowie, E. J., Keene, D. R., Stripp, B. R., Randell, S. H., Noble, P. W. and Hogan, B. L. M. (2013). Type 2 alveolar cells are stem cells in adult lung. *J. Clin. Invest.* **123**, 3025-3036.
Bhatt, A. J., Pryhuber, G. S., Huyck, H., Watkins, R. H., Metlay, L. A. and Maniscalco, W. M. (2001). Disrupted pulmonary vasculature and decreased vascular endothelial growth factor, Flt-1, and TIE-2 in human infants dying with bronchopulmonary dysplasia. *Am. J. Respir. Crit. Care Med.* **164**, 1971-1980.
Birdsey, G. M., Shah, A. V., Dufton, N., Reynolds, L. E., Osuna Almagro, L., Yang, Y., Aspalter, I. M., Khan, S. T., Mason, J. C., Dejana, E. et al. (2015). The endothelial transcription factor ERG promotes vascular stability and growth through Wnt/beta-catenin signaling. *Dev. Cell* **32**, 82-96.
Borok, Z., Liebler, J. M., Lubman, R. L., Foster, M. J., Zhou, B., Li, X., Zabski, S. M., Kim, K. J. and Crandall, E. D. (2002). Na transport proteins are expressed by rat alveolar epithelial type I cells. *Am. J. Physiol. Lung Cell Mol. Physiol.* **282**, L599-L608.
Burri, P. H. (1984). Fetal and postnatal development of the lung. *Annu. Rev. Physiol.* **46**, 617-628.
Chang, D. R., Martinez Alanis, D., Miller, R. K., Ji, H., Akiyama, H., McCrea, P. D. and Chen, J. (2013). Lung epithelial branching program antagonizes alveolar differentiation. *Proc. Natl. Acad. Sci. USA* **110**, 18042-18051.
Chen, Y., Shi, L., Zhang, L., Li, R., Liang, J., Yu, W., Sun, L., Yang, X., Wang, Y., Zhang, Y. et al. (2008). The molecular mechanism governing the oncogenic potential of SOX2 in breast cancer. *J. Biol. Chem.* **283**, 17969-17978.
Crapo, J. D., Barry, B. E., Gehr, P., Bachofen, M. and Weibel, E. R. (1982). Cell number and cell characteristics of the normal human lung. *Am. Rev. Respir. Dis.* **126**, 332-337.
Danto, S. I., Shannon, J. M., Borok, Z., Zabski, S. M. and Crandall, E. D. (1995). Reversible transdifferentiation of alveolar epithelial cells. *Am. J. Respir. Cell Mol. Biol.* **12**, 497-502.
Dassule, H. R., Lewis, P., Bei, M., Maas, R. and McMahon, A. P. (2000). Sonic hedgehog regulates growth and morphogenesis of the tooth. *Development* **127**, 4775-4785.
Desai, T. J., Brownfield, D. G. and Krasnow, M. A. (2014). Alveolar progenitor and stem cells in lung development, renewal and cancer. *Nature* **507**, 190-194.
Flodby, P., Borok, Z., Banfalvi, A., Zhou, B., Gao, D., Minoo, P., Ann, D. K., Morrisey, E. E. and Crandall, E. D. (2010). Directed expression of Cre in alveolar epithelial type 1 cells. *Am. J. Respir. Cell Mol. Biol.* **43**, 173-178.
Gontan, C., de Munck, A., Vermeij, M., Grosveld, F., Tibboel, D. and Rottier, R. (2008). Sox2 is important for two crucial processes in lung development: branching morphogenesis and epithelial cell differentiation. *Dev. Biol.* **317**, 296-309.
Gonzalez, R., Yang, Y. H., Griffin, C., Allen, L., Tigue, Z. and Dobbs, L. (2005). Freshly isolated rat alveolar type I cells, type II cells, and cultured type II cells have distinct molecular phenotypes. *Am. J. Physiol. Lung Cell. Mol. Physiol.* **288**, L179-L189.
Gonzalez, R. F., Allen, L. and Dobbs, L. G. (2009). Rat alveolar type I cells proliferate, express OCT-4, and exhibit phenotypic plasticity in vitro. *Am. J. Physiol. Lung Cell. Mol. Physiol.* **297**, L1045-L1055.
Halai, K., Whiteford, J., Ma, B., Nourshargh, S. and Woodfin, A. (2014). ICAM-2 facilitates luminal interactions between neutrophils and endothelial cells in vivo. *J. Cell Sci.* **127**, 620-629.
Harfe, B. D., Scherz, P. J., Nissim, S., Tian, H., McMahon, A. P. and Tabin, C. J. (2004). Evidence for an expansion-based temporal Shh gradient in specifying vertebrate digit identities. *Cell* **118**, 517-528.
Herzog, E. L., Brody, A. R., Colby, T. V., Mason, R. and Williams, M. C. (2008). Knowns and unknowns of the alveolus. *Proc. Am. Thorac. Soc.* **5**, 778-782.
Hsia, C. C. W., Hyde, D. M., Ochs, M., Weibel, E. R. and **on behalf of the ATS/ERS Joint Task Force on the Quantitative Assessment of Lung Structure** (2010). An official research policy statement of the American Thoracic Society/European Respiratory Society: standards for quantitative assessment of lung structure. *Am. J. Respir. Crit. Care Med.* **181**, 394-418.
Ikeda, K., Clark, J. C., Shaw-White, J. R., Stahlman, M. T., Boutell, C. J. and Whitsett, J. A. (1995). Gene structure and expression of human thyroid transcription factor-1 in respiratory epithelial cells. *J. Biol. Chem.* **270**, 8108-8114.
Jain, R., Barkauskas, C. E., Takeda, N., Bowie, E. J., Aghajanian, H., Wang, Q., Padmanabhan, A., Manderfield, L. J., Gupta, M., Li, D. et al. (2015). Plasticity of Hopx(+) type I alveolar cells to regenerate type II cells in the lung. *Nat. Commun.* **6**, 6727.
Johnson, M. D., Widdicombe, J. H., Allen, L., Barbry, P. and Dobbs, L. G. (2002). Alveolar epithelial type I cells contain transport proteins and transport sodium, supporting an active role for type I cells in regulation of lung liquid homeostasis. *Proc. Natl. Acad. Sci. USA* **99**, 1966-1971.
Johnson, M. D., Bao, H.-F., Helms, M. N., Chen, X.-J., Tigue, Z., Jain, L., Dobbs, L. G. and Eaton, D. C. (2006). Functional ion channels in pulmonary alveolar type I cells support a role for type I cells in lung ion transport. *Proc. Natl. Acad. Sci. USA* **103**, 4964-4969.
Kasahara, Y., Tuder, R. M., Taraseviciene-Stewart, L., Le Cras, T. D., Abman, S., Hirth, P. K., Waltenberger, J. and Voelkel, N. F. (2000). Inhibition of VEGF receptors causes lung cell apoptosis and emphysema. *J. Clin. Invest.* **106**, 1311-1319.
Kauffman, S. L., Burri, P. H. and Weibel, E. R. (1974). The postnatal growth of the rat lung. II. Autoradiography. *Anat. Rec.* **180**, 63-76.
Kim, D., Pertea, G., Trapnell, C., Pimentel, H., Kelley, R. and Salzberg, S. L. (2013). TopHat2: accurate alignment of transcriptomes in the presence of insertions, deletions and gene fusions. *Genome Biol.* **14**, R36.
Kimura, T., Kawabe, H., Jiang, C., Zhang, W., Xiang, Y.-Y., Lu, C., Salter, M. W., Brose, N., Lu, W.-Y. and Rotin, D. (2011). Deletion of the ubiquitin ligase Nedd4L in lung epithelia causes cystic fibrosis-like disease. *Proc. Natl. Acad. Sci. USA* **108**, 3216-3221.
Kuhn, C. (1988). Biotin stores in rodent lungs: localization to Clara and type II alveolar cells. *Exp. Lung Res.* **14**, 527-536.
Kumar, M. E., Bogard, P. E., Espinoza, F. H., Menke, D. B., Kingsley, D. M. and Krasnow, M. A. (2014). Mesenchymal cells. Defining a mesenchymal progenitor niche at single-cell resolution. *Science* **346**, 1258810.
Langmead, B. and Salzberg, S. L. (2012). Fast gapped-read alignment with Bowtie 2. *Nat. Methods* **9**, 357-359.
Lu, Y., Futtner, C., Rock, J. R., Xu, X., Whitworth, W., Hogan, B. L. M. and Onaitis, M. W. (2010). Evidence that SOX2 overexpression is oncogenic in the lung. *PLoS ONE* **5**, e11022.
Madisen, L., Zwingman, T. A., Sunkin, S. M., Oh, S. W., Zariwala, H. A., Gu, H., Ng, L. L., Palmiter, R. D., Hawrylycz, M. J., Jones, A. R. et al. (2010). A robust and high-throughput Cre reporting and characterization system for the whole mouse brain. *Nat. Neurosci.* **13**, 133-140.
Maeda, Y., Tsuchiya, T., Hao, H., Tompkins, D. H., Xu, Y., Mucenski, M. L., Du, L., Keiser, A. R., Fukazawa, T., Naomoto, Y. et al. (2012). Kras(G12D) and Nkx2-1 haploinsufficiency induce mucinous adenocarcinoma of the lung. *J. Clin. Invest.* **122**, 4388-4400.
Muzumdar, M. D., Tasic, B., Miyamichi, K., Li, L. and Luo, L. (2007). A global double-fluorescent Cre reporter mouse. *Genesis* **45**, 593-605.
Ng, Y.-S., Rohan, R., Sunday, M. E., Demello, D. E. and D'Amore, P. A. (2001). Differential expression of VEGF isoforms in mouse during development and in the adult. *Dev. Dyn.* **220**, 112-121.
Prigge, J. R., Wiley, J. A., Talago, E. A., Young, E. M., Johns, L. L., Kundert, J. A., Sonsteng, K. M., Halford, W. P., Capecchi, M. R. and Schmidt, E. E. (2013). Nuclear double-fluorescent reporter for in vivo and ex vivo analyses of biological transitions in mouse nuclei. *Mamm. Genome* **24**, 389-399.
Que, J., Luo, X., Schwartz, R. J. and Hogan, B. L. (2009). Multiple roles for Sox2 in the developing and adult mouse trachea. *Development* **136**, 1899-1907.
Rawlins, E. L., Clark, C. P., Xue, Y. and Hogan, B. L. M. (2009). The Id2+ distal tip lung epithelium contains individual multipotent embryonic progenitor cells. *Development* **136**, 3741-3745.
Roberts, A., Pimentel, H., Trapnell, C. and Pachter, L. (2011a). Identification of novel transcripts in annotated genomes using RNA-Seq. *Bioinformatics* **27**, 2325-2329.
Roberts, A., Trapnell, C., Donaghey, J., Rinn, J. L. and Pachter, L. (2011b). Improving RNA-Seq expression estimates by correcting for fragment bias. *Genome Biol.* **12**, R22.
Scherle, W. (1970). A simple method for volumetry of organs in quantitative stereology. *Mikroskopie* **26**, 57-60.

Development (2016) 143, 54-65 doi:10.1242/dev.130005

Schittny, J. C., Djonov, V., Fine, A. and Burri, P. H. (1998). Programmed cell death contributes to postnatal lung development. *Am. J. Respir. Cell Mol. Biol.* **18**, 786-793.

Shioi, G., Kiyonari, H., Abe, T., Nakao, K., Fujimori, T., Jang, C.-W., Huang, C.-C., Akiyama, H., Behringer, R. R. and Aizawa, S. (2011). A mouse reporter line to conditionally mark nuclei and cell membranes for in vivo live-imaging. *Genesis* **49**, 570-578.

Snippert, H. J., van der Flier, L. G., Sato, T., van Es, J. H., van den Born, M., Kroon-Veenboer, C., Barker, N., Klein, A. M., van Rheenen, J., Simons, B. D. et al. (2010). Intestinal crypt homeostasis results from neutral competition between symmetrically dividing Lgr5 stem cells. *Cell* **143**, 134-144.

Snyder, E. L., Watanabe, H., Magendantz, M., Hoersch, S., Chen, T. A., Wang, D. G., Crowley, D., Whittaker, C. A., Meyerson, M., Kimura, S. et al. (2013). Nkx2-1 represses a latent gastric differentiation program in lung adenocarcinoma. *Mol. Cell* **50**, 185-199.

Soeda, T., Deng, J. M., de Crombrugghe, B., Behringer, R. R., Nakamura, T. and Akiyama, H. (2010). Sox9-expressing precursors are the cellular origin of the cruciate ligament of the knee joint and the limb tendons. *Genesis* **48**, 635-644.

Stenmark, K. R. and Abman, S. H. (2005). Lung vascular development: implications for the pathogenesis of bronchopulmonary dysplasia. *Annu. Rev. Physiol.* **67**, 623-661.

Stone, K. C., Mercer, R. R., Gehr, P., Stockstill, B. and Crapo, J. D. (1992). Allometric relationships of cell numbers and size in the mammalian lung. *Am. J. Respir. Cell Mol. Biol.* **6**, 235-243.

Takeda, N., Jain, R., LeBoeuf, M. R., Wang, Q., Lu, M. M. and Epstein, J. A. (2011). Interconversion between intestinal stem cell populations in distinct niches. *Science* **334**, 1420-1424.

Taniguchi, H., He, M., Wu, P., Kim, S., Paik, R., Sugino, K., Kvitsiani, D., Fu, Y., Lu, J., Lin, Y. et al. (2011). A resource of Cre driver lines for genetic targeting of GABAergic neurons in cerebral cortex. *Neuron* **71**, 995-1013.

Tompkins, D. H., Besnard, V., Lange, A. W., Wert, S. E., Keiser, A. R., Smith, A. N., Lang, R. and Whitsett, J. A. (2009). Sox2 is required for maintenance and differentiation of bronchiolar Clara, ciliated, and goblet cells. *PLoS ONE* **4**, e8248.

Tompkins, D. H., Besnard, V., Lange, A. W., Keiser, A. R., Wert, S. E., Bruno, M. D. and Whitsett, J. A. (2011). Sox2 activates cell proliferation and differentiation in the respiratory epithelium. *Am. J. Respir. Cell Mol. Biol.* **45**, 101-110.

Trapnell, C., Roberts, A., Goff, L., Pertea, G., Kim, D., Kelley, D. R., Pimentel, H., Salzberg, S. L., Rinn, J. L. and Pachter, L. (2012). Differential gene and transcript expression analysis of RNA-seq experiments with TopHat and Cufflinks. *Nat. Protoc.* **7**, 562-578.

Trapnell, C., Hendrickson, D. G., Sauvageau, M., Goff, L., Rinn, J. L. and Pachter, L. (2013). Differential analysis of gene regulation at transcript resolution with RNA-seq. *Nat. Biotechnol.* **31**, 46-53.

Treutlein, B., Brownfield, D. G., Wu, A. R., Neff, N. F., Mantalas, G. L., Espinoza, F. H., Desai, T. J., Krasnow, M. A. and Quake, S. R. (2014). Reconstructing lineage hierarchies of the distal lung epithelium using single-cell RNA-seq. *Nature* **509**, 371-375.

Tschanz, S. A., Burri, P. H. and Weibel, E. R. (2011). A simple tool for stereological assessment of digital images: the STEPanizer. *J. Microsc.* **243**, 47-59.

Van Keymeulen, A., Mascre, G., Youseff, K. K., Harel, I., Michaux, C., De Geest, N., Szpalski, C., Achouri, Y., Bloch, W., Hassan, B. A. et al. (2009). Epidermal progenitors give rise to Merkel cells during embryonic development and adult homeostasis. *J. Cell Biol.* **187**, 91-100.

Van Keymeulen, A., Rocha, A. S., Ousset, M., Beck, B., Bouvencourt, G., Rock, J., Sharma, N., Dekoninck, S. and Blanpain, C. (2011). Distinct stem cells contribute to mammary gland development and maintenance. *Nature* **479**, 189-193.

Weibel, E. R. (1971). The mystery of “non-nucleated plates” in the alveolar epithelium of the lung explained. *Cells Tissues Organs* **78**, 425-443.

Weibel, E. R. (2015). On the tricks alveolar epithelial cells play to make a good lung. *Am. J. Respir. Crit. Care Med.* **191**, 504-513.

Williams, M. C. (2003). Alveolar type I cells: molecular phenotype and development. *Annu. Rev. Physiol.* **65**, 669-695.

Williams, R. W. and Rakic, P. (1988). Three-dimensional counting: an accurate and direct method to estimate numbers of cells in sectioned material. *J. Comp. Neurol.* **278**, 344-352.

Winslow, M. M., Dayton, T. L., Verhaak, R. G. W., Kim-Kiselak, C., Snyder, E. L., Feldser, D. M., Hubbard, D. D., DuPage, M. J., Whittaker, C. A., Hoersch, S. et al. (2011). Suppression of lung adenocarcinoma progression by Nkx2-1. *Nature* **473**, 101-104.

Yang, J. and Chen, J. (2014). Developmental programs of lung epithelial progenitors: a balanced progenitor model. *Wiley Interdiscip. Rev. Dev. Biol.* **3**, 331-347.

Zhou, L., Lim, L., Costa, R. H. and Whitsett, J. A. (1996). Thyroid transcription factor-1, hepatocyte nuclear factor-3beta, surfactant protein B, C, and Clara cell secretory protein in developing mouse lung. *J. Histochem. Cytochem.* **44**, 1183-1193.